Acta Materialia 118 (2016) 187–195

Contents lists available at ScienceDirect

Acta Materialia

journal homepage: www.elsevier.com/locate/actamat

Full length article

# Improving the mechanical properties of Fe – $TiB_2$ high modulus steels through controlled solidification processes

H. Zhang, H. Springer*, R. Aparicio-Fernández, D. Raabe

*Max-Planck-Institut für Eisenforschung GmbH, 40237 Düsseldorf, Germany*

ARTICLE INFO

*Article history:*
Received 4 July 2016
Received in revised form
25 July 2016
Accepted 28 July 2016

*Keywords:*
Steel
Young's modulus
Density
Ductility
Strength
Toughness

ABSTRACT

We investigated novel pathways to improve the mechanical properties of liquid metallurgy produced Fe – $TiB_2$ based high modulus steels (HMS) by controlled solidification kinetics and subsequent thermo-mechanical treatments. The solidification rate was varied by casting of hyper-eutectic alloys (20 vol% $TiB_2$) into moulds with differing internal thickness. Ingots between 5 and 40 mm thickness exhibited irregular particle microstructure consisting of sharp-edged coarse primary particles (increasingly clustered with slower solidification) and closely spaced irregular lamellae. Casting defects can be alleviated by hot rolling, but the mechanical properties remain unsatisfactory. Increasing the solidification rate results only at mould thicknesses of 4 mm and below in a significant refinement of the particle microstructure, necessitating liquid metal deposition techniques to utilise it for obtained improved mechanical performance of HMS. Decreasing the solidification rate causes density-induced floatation of the primary particles, which can be used in block-casting for the production of alloys consisting of small and spheroidised eutectic particles, exhibiting high ductility and superior toughness. Annealing just above the solidus-temperature allows the eutectic zones to liquefy and sink, leaving only primary $TiB_2$ particles behind in the top zone of the alloy. Despite the increased particle fraction up to 24 vol%, both strength, specific modulus and ductility are improved over standard processed HMS alloys with 20 vol% $TiB_2$.



## 1. Introduction

Steels represent the most common and successful structural materials due to their unprecedented spectrum of mechanical and physical properties. Current steel design studies pursue multiple directions, for example for further improving corrosion [1] and wear resistance [2], high temperature stability [3] and energy absorption [4]. For lightweight design such as required in transportation systems, the major challenge lies in increasing strength and reducing the density (ρ). Only recently, also stiffness (i.e. the Young's modulus; $E$) is being considered as a design criterion, as an increased specific modulus (i.e. $E/\rho$) – above the typical value of about 26 GPa $g^{-1}$ $cm^3$ for steels, aluminium (Al), magnesium (Mg) and titanium (Ti) alloys – offers utilising yet untapped potential in lightweight materials design [5]. For this purpose, so called high modulus steels (HMS) have been developed, i.e. iron (Fe) based metal-matrix-composites, which allow to blend lightweight and stiff phases with strong, ductile, tough, and not the least cost effective steel matrices [6,7].

In this light, the Fe – Ti-diboride ($TiB_2$) system has received considerable attention. $TiB_2$ is not only very effective ($E$ ~ 565 GPa, ρ ~ 4.25 g $cm^{-3}$ [8]), but also allows for volume production of HMS via liquid metallurgical synthesis methods, as $TiB_2$ – unlike for example most oxides or nitrides – can be precipitated from a homogenous Fe – Ti – B melt in a pseudo-binary eutectic reaction [9] (Fig. 1a). Furthermore, interface analyses at the atomic scale revealed a strong interfacial cohesion between Fe and TiB2 particles [10]. According to theoretical predictions, i.e. a rule of mixture for ρ and the Halpin-Tsai model for $E$ [10], respectively, the specific modulus increases with the $TiB_2$ fraction to about 37 GPa $g^{-1}$ $cm^3$ for 30 vol % $TiB_2$ (Fig. 1b). However, if the $TiB_2$ fraction rises above 12 vol% (~6.3 mol.%), the alloy is above the eutectic $TiB_2$ concentration (Fig. 1a), and as a consequence, mechanically unfavourable $TiB_2$-morphologies result; i.e. coarse particles stemming from primary solidification additional to the already sharp-edged lamellae from the eutectic decomposition [6,7]. Additionally, the $TiB_2$ particles are rather brittle ($K_{IC}$ of $TiB_2$ ~ 5 MPa $m^{1/2}$ [8]) and their

* Corresponding author.
*E-mail address:* h.springer@mpie.de (H. Springer).

http://dx.doi.org/10.1016/j.actamat.2016.07.056
1359-6454/

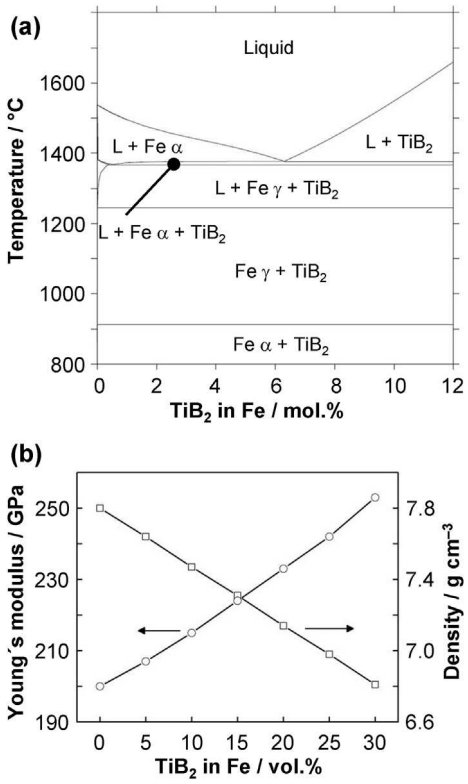


**Fig. 1.** (a) Phase diagram of the pseudo-binary Fe–$TiB_2$ system calculated with Thermocalc. (b) Prediction of Young's modulus (Halpin-Tsai model [10]) and density (rule of mixture) of Fe for different volume fractions of $TiB_2$.

elevated stiffness induces stress concentration at the interface with the steel matrix. All this together causes pronounced embrittlement of the bulk material with increasing particle fractions, i.e. a deterioration of the mechanical performance with improvement of the physical properties.

One promising pathway to improve the ductility of HMS is to utilise alloying additions in order to modify the constitution and mechanical performance of the steel matrix, exceeding the properties of a pure Fe reference matrix (i.e. ferrite) towards stronger and more ductile multiphase microstructures well known from advanced high strength steel concepts [11,12]. The effect of the alloying additions on the particles' morphology is limited though [13], and thus the challenge remains to achieve a more mechanically compliant $TiB_2$ shape, size and dispersion. As the $TiB_2$ particles represent solidification products and are thermodynamically stable in the solid HMS, their morphology can not be significantly influenced through dissolving and re-precipitation processes, as it is commonly applied for example with alloy carbides in tool steels [14]. Thermo-mechanical treatments (TMT; i.e. hot and cold rolling) have been reported to have pronounced effects on the HMS microstructure, namely, inducing plastic deformation of the particles in case of hot rolling [15] as well as their fragmentation [16,17]. The latter phenomenon leads to embrittlement of the material and reduces its stiffness [17]. However, we recently demonstrated how $TiB_2$ particles can be effectively influenced by controlling the solidification rate of HMS melts, thereby refining the particles shape away from irregularly sharp-edges to spheres, as well as reducing their sizes by several orders of magnitude down to the nanometre range [6]. Especially the density-induced separation of primary and eutectic particles, observed for very slow cooling conditions [6], is extremely promising, as it can be utilised for the efficient production of large quantities of HMS under industrially controllable conditions. While these processes can be readily combined with the aforementioned alloy design of the steel matrix in a later stage, their extent and thus the cost and associated processing efforts may be reduced to achieve HMS with superior physical and mechanical property profiles.

## 2. Objective

The objective of this work is to systematically study how the inverse relationship between mechanical and physical properties of Fe – $TiB_2$ based HMS can be overcome by tailored solidification processes. We aim at developing processing guidelines to obtain high particle fractions to increase the specific modulus without sacrificing the material's ductility and toughness, suitable for volume production and as the basis for the alloy design of HMS.

## 3. Materials and methods

### 3.1. Synthesis and processing

All alloys in this study were of the nominal composition Fe – 10.10 Ti – 3.86 B (wt.%; corresponding to a hypereutectic concentration with ~20 vol% $TiB_2$), and were prepared by melting pure metals in a vacuum induction furnace (VIM) under an argon (Ar) atmosphere. The Ti content was chosen about 17% over the stoichiometric amount required for $TiB_2$ (resulting in about 1.9 wt% Ti in the ferritic matrix) in order to suppress the formation of Fe-borides and to neutralise any inadvertently present carbon by the formation of Ti-carbides [19]. TiC carbides were found to precipitate in epitaxy with the basal plane of TiB2 particles [10]. The solidification rate was varied by the internal thickness of rectangular water-cooled copper (Cu) moulds from 40 mm down to 1 mm (all moulds 40 mm wide), increasing the solidification rate with decreasing ingot thickness. As moulds with an internal thickness below 1 mm could not be filled reliably with liquid metal, even more rapid solidification was achieved by melt spinning: Charges of about 10 g, cut from the 10 mm thick VIM samples, were molten at 1600 °C in a boron nitride crucible and ejected through the slit-nozzle with an Ar pressure of 300 mbar onto a water-cooled Cu wheel rotating at a tangential velocity of 10 m $s^{-1}$, rendering ribbons of 100–500 μm thickness. The cooling rate for 20 mm thick VIM casts was measured to be about 10 K $s^{-1}$ [6], whereas during melt spinning ~ $10^5$ K $s^{-1}$ can be achieved [20]. Hot rolling followed by air cooling was performed on selected materials at 1100 °C to a final thickness of 2 and 6 mm, respectively.

In order to investigate the density-induced separation of primary and eutectic particles in more detail, samples from 10 mm thick VIM ingots were reheated to various temperatures between 1250 and 1640 °C. Critical temperatures of the alloy (e.g. transition, solidus and liquidus temperatures) and corresponding microstructures were determined by differential scanning calorimetry measurements (DSC; NETZSCH 404C) and differential thermal analysis (DTA; Setaram SETSYS-1750). DSC and DTA experiments were performed with cylindrical samples (3 mm diameter, 3 mm long), placed in alumina crucibles under Ar atmosphere, heated and cooled at 1 K $min^{-1}$ (no holding time at temperature). The first and second order transitions were revealed by the extrapolated peak-onset temperatures [21,22].

### 3.2. Characterisation and testing

Microstructures were characterised with a field emission scanning electron microscope (SEM; JEOL-6500F, operated at 15 kV) for imaging and electron backscatter diffraction analysis (EBSD; step size 50 nm, TSL OIM analysis software). ImageJ software was used

to quantify the size of particles on six backscatter electron images (BSE) at 3000 magnification. *E* values were measured by a sonic excitation system (flexural vibration resonance, model MK5 "Industrial") on cylindrical specimens (6 mm diameter, 40 mm long, axis parallel to the rolling direction), using a rule of mixture for the Poisson-ratio of our composite material in order to calculate *E* from the measured reduced *E* values. The ρ values were determined by the Archimedes method (micromeritics AccuPyc 1330, under Ar). Tensile tests were conducted using dog bone-shaped flat tensile samples (gauge length 5 mm, tensile axis parallel to the rolling direction for hot rolled samples) at a constant crosshead speed of 5 μm $s^{-1}$, corresponding to an initial strain rate of $10^{-3}$ $s^{-1}$. Digital image correlation analysis (DIC, Aramis software produced by GOM GmbH) was conducted to obtain engineering strain/stress curves. Impact toughness tests were performed at room temperature on mini-Charpy samples (27 × 3 × 4 $mm^3$, 60° V-notch). All given values represent the average of three tests each, respectively.

## 4. Results

### 4.1. Increasing the solidification rate

Fig. 2a shows the microstructure of a hyper-eutectic Fe – $TiB_2$ HMS alloy in the as-cast state for 40 mm thick ingot, as it is characteristic for solidification close to industrial conditions [6]. SE images at different magnifications reveal coarse, blocky primary particles (about 10 μm in diameter, mostly clustered together) and fine eutectic particles of irregular shape, as well as typical casting defects such as pores (white arrows in Fig. 2a). According to the EBSD inverse pole figure map (IPF; with high angle grain boundaries 15–62.8° superimposed) the grain size of the ferritic matrix is about 19 μm. The ferritic matrix contains with about 1.3 wt% Ti slightly less Ti than expected from the targeted values. After hot-rolling (Fig. 2b) the morphology and dispersion of the primary particles is not changed significantly, while the eutectic particles have been spheroidised to some extent, i.e. are of less sharp-cornered morphology with a smaller aspect ratio. The matrix grain size is reduced by hot-rolling to about 11 μm and the casting pores are closed, but some of the primary $TiB_2$ particles – especially those which have been clustered together – now exhibit cracks (white arrow in Fig. 2b). Nevertheless, the tensile performance of the HMS alloy (Fig. 2c) is improved significantly through hot-rolling, as yield strength (YS) increases from ~200 MPa to 350 MPa, ultimate tensile strength (UTS) from ~500 MPa to ~ 650 MPa, and the total elongation (TE) from less than 3% to more than 7%. Measurements of *E* and ρ in the as-cast state were affected by the aforementioned porosity and could not be reliably performed, whereas the hot-rolled material exhibited values of *E* ~243 GPa and ρ ~7.2 g $cm^{-3}$, which is in reasonable agreement with the predicted values (Fig. 1b) in view of the notorious difficulties in measuring materials stiffness data [23].

Investigations of the fracture behaviour, i.e. SEM analysis close to the fractured surface of a ruptured tensile sample (here shown on the example of the 40 mm thick as-cast material, Fig. 3), reveal a complex scenario: SEM images and EBSD analysis from a longitudinal section of a fractured sample (Fig. 3a and b) and the fractured surface (Fig. 3c) show that most of the primary and some of the eutectic particles are cracked, and it appears that cracks probably propagate preferably along the {100} planes of ferrite grains. However, no clear conclusion can be drawn regarding the dominant factors for crack initiation and propagation, such as interfacial delamination, crack path percolation or high mechanical contrast across interfaces [24–26].

The effect of an increased solidification rate, i.e. a decreased mould size, on the size of primary and eutectic $TiB_2$ particles as well

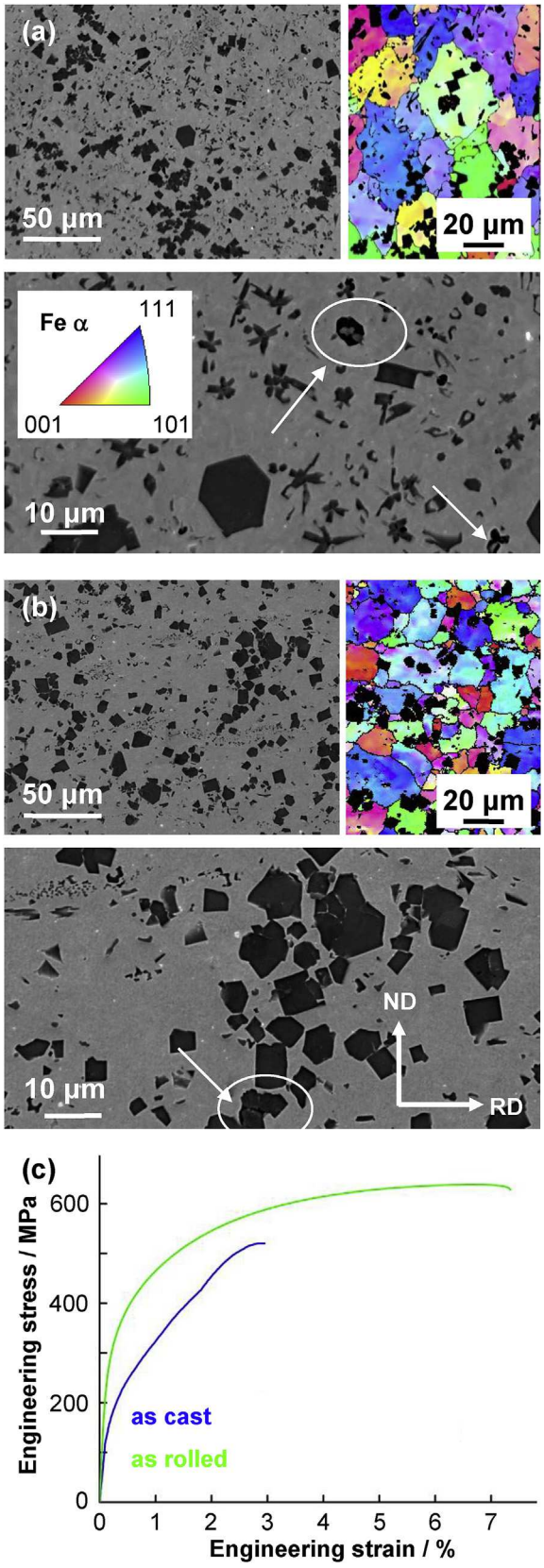


**Fig. 2.** Characterisation results for a High Modulus Steel with 20 vol% $TiB_2$ cast into a 40 mm thick mould: SEM images and EBSD IPF maps for the as-cast (a) and hot-rolled state (b), and tensile curves for both states (c). The white arrows and circles in (a) and (b) highlight pores and cracks, respectively.

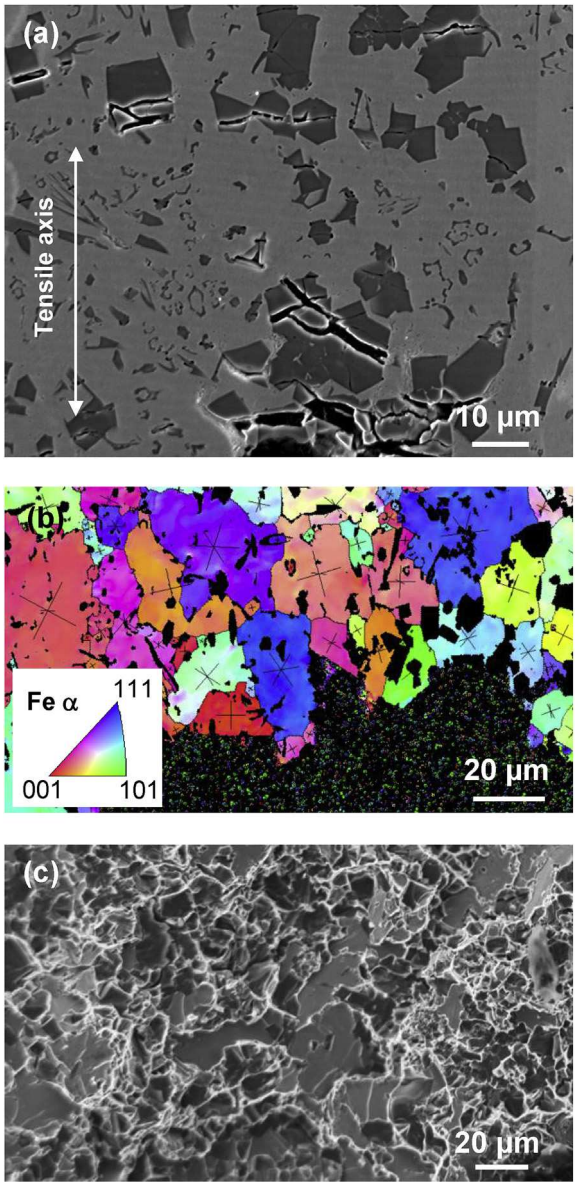


**Fig. 3.** Analysis of the fracture behaviour of a High Modulus Steel with 20 vol% $TiB_2$ cast into a 40 mm thick mould after hot rolling: SEM image (a) and EBSD IPF map (b) of a longitudinal section close to the fracture zone, and SEM image of the fractured surface (c).

as on the ferritic matrix grains is shown in Fig. 4 (all in the as-cast state). Particles of a size smaller than 10 $\mu m^2$ were counted as eutectic constituents, larger ones as primary particles. This criterion was chosen because their differentiation for a statistical analysis is difficult, due to the irregular shape of the eutectic and the aforementioned agglomeration of primary particles. As shown in Fig. 4a and b, average values and scatter of both, matrix grains and $TiB_2$ particles, are only slightly affected by decreasing the mould thickness from 40 down to 10 mm. Further increasing the solidification rate by a mould thickness of 1 mm leads to a refinement of the primary (average size from about 50 down to 25 $\mu m^2$) and the eutectic particles (from about 0.8 to 0.1 $\mu m^2$), while the grains of the ferritic matrix decrease in diameter from about 16 to 4 μm and become more and more globular from their dendritic origin (Fig. 4c). With even faster solidification, i.e. in meltspun ribbons, the formation of eutectic particles is suppressed at ribbon-thicknesses below about 200 μm, while primary particles can be still observed even at the fastest solidified samples, i.e. in ribbons with a thickness of about 100 μm (Fig. 4d).

The effects of hot rolling on HMS produced with an accelerated solidification rate are exemplified in Fig. 5 on 4 mm thick material. SEM analysis (Fig. 5a) revealed that casting defects – already minimised by the accelerated solidification – are cured, but agglomerated primaries were cracked by the induced deformation, similar to the results for thicker ingots (Fig. 2). The already small matrix grain size was only slightly reduced from about 8 to 7 μm by hot rolling. The inhomogeneous size distribution and the sub-grain boundaries inside the larger grains indicate that the chosen hot rolling parameters did not result in to complete recrystallisation of the matrix. While hot rolling again improved the resultant tensile properties compared to the as-cast state, YS, UTS and TE are very similar to the values obtained for hot rolled material stemming from slower solidification (Fig. 5b). The microstructure refinement induced by the accelerated solidification did not translate into enhanced mechanical properties.

### *4.2. Decreasing the solidification rate and exploiting the density-induced phase separation*

Fig. 6 shows the DTA results for reheating a sample stemming from a 10 mm thick ingot up to 1640 °C with a heating and cooling rate of 1 K $min^{-1}$, which is much slower than those of the VIM experiments (about 10 K $s^{-1}$ for 20 mm ingot thickness [6]). The heating curve (red) exhibits a sharp peak at 1320 °C and three less pronounced peaks at 780 °C, 1090 °C and 1596 °C, respectively. The sharp peak at 1320 °C is attributed to the solid-liquid transition. The peak at 780 °C corresponds with the ferromagnetic-paramagnetic transition of α-Fe; the one at 1090 °C to the α/γ transformation temperature of Fe being increased from 910 °C (in pure Fe) by the Ti solutes. The peak at 1596 °C appears to be related to the completed liquefaction, i.e. dissolution of the last remaining (primary) $TiB_2$ particles. The shifting of the temperatures of the corresponding peaks on the cooling curve (blue) and the appearance of an additional peak close to the liquid-solid transition suggests a different composition profile during cooling as compared to that during heating. The small kinks at around 1430 °C are no pronounced peaks, but most probably artefacts caused by the measurement setup. The difference between our experimentally derived values and those of the calculated Fe – $TiB_2$ phase diagram (Fig. 1a) appear reasonable in view of the still not unambiguously defined thermodynamic phenomena and the non-equilibrium conditions of our DSC/DTA setup.

The corresponding microstructures after reheating and slow cooling of HMS (DTA samples; no holding time at maximum temperature) are shown in the SEM pictures compiled in Fig. 7. After annealing at 1250 °C, i.e. just below the onset of melting, no pronounced changes compared to the typical as-cast condition can be observed, except for a spheroidisation of the eutectic lamellae. After annealing just above the solidus-temperature (at 1320 °C), however, two distinct zones can now be observed. While the bottom quarter of the sample now consists exclusively of – again mainly spheroidised – eutectic lamellae, only few of them are found in the top between the remaining primary particles. In a sample annealed at 1450 °C, the size of the purely eutectic zone at the bottom grows to about 40 vol%, the particle fraction in the top zone increases. In between the two zones a distinct line of $TiB_2$ particles can be found now, whose morphology resembles those stemming from primary solidification, but their grain size is larger than of those found in the top zone. This trend increases with the annealing temperature to 1550 °C (just below the liquidus-temperature), i.e. as the bottom zone grows, the particle fraction in the top zone increases, as well as the grain size of the particles in between the two zones. After

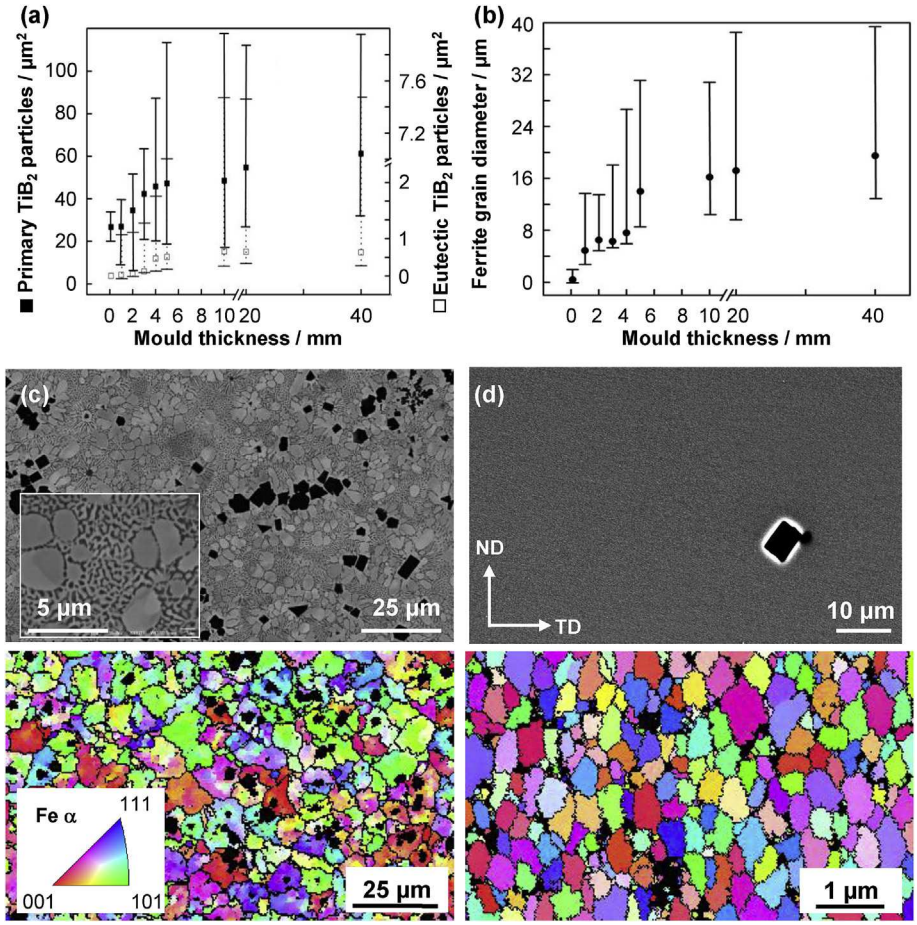


**Fig. 4.** Effect of the ingot thickness and thus solidification rate on the microstructure of High Modulus Steels with 20 vol% $TiB_2$: (a) Size of primary and eutectic $TiB_2$ particles and (b) grain size of the ferritic matrix, both as a function of the mould thickness. Exemplary SEM images and EBSD IPF maps for casting into a 1 mm thick mould (c) and from 0.1 mm thick melt spun ribbon (d).

annealing above the liquidus-temperature (1640 °C), the eutectic zone takes up the entire sample, only at the very top extremely large primary $TiB_2$ particles are found.

The mechanical and physical characterisation of the two distinct microstructure zones induced by annealing the HMS above the solidus-temperature requires larger samples as those used in the DTA/DSC experiments. Thus, respective larger samples were produced from 100 mm long sections of a 10 mm thick ingot, packed into ceramic crucibles with alumina powder, annealed for 30 min under Ar at 1450 °C and cooled to room temperature at 10 K $min^{-1}$. Afterwards they were hot rolled at 1100 °C in order to reduce any possible solidification-induced defects (Fig. 2a). Results for the top zone (top of Fig. 8a) show that the chosen parameters did not result in a complete removal of eutectic particles as in the DTA specimens. The few remaining ones, however, are almost fully spheroidised, and the particle's morphology and dispersion appears to be of much higher mechanical compliance to the matrix than those obtained from standard casting and hot rolling (Fig. 2b). Indeed, the corresponding tensile strength and ductility (bottom of Fig. 8a) are improved, despite of the higher particle fraction (24 vol% $TiB_2$) and consequently enhanced physical properties ($E$ ~ 249 GPa and $\rho$ ~ 7.0 g $cm^{-3}$) compared to a standard processed HMS with 20 vol% $TiB_2$ ($E$ ~ 243 GPa, $\rho$ ~ 7.2 g $cm^{-3}$). The grain size of the ferrite matrix is due to the comparatively long annealing at high temperature with 20 µm larger than those of conventionally cast and hot rolled sample (Fig. 2b), whereas the toughness is with 1.92 J $cm^{-2}$ opposed to 2.76 J $cm^{-2}$ slightly lower. The bottom region of the annealed and hot rolled sample (Fig. 8b) consists on the other hand, as the respective DSC samples, completely of spheroidised eutectic $TiB_2$ particles in the ferrite matrix. Due to the decreased particle fraction (about 12 vol%) both tensile strength (~510 MPa) and $E$ (~225 GPa) are lower, but tensile ductility (~25%) and $\rho$ (~7.4 g $cm^{-3}$) are higher than the alloys containing 20 and 24 vol% $TiB_2$, respectively. Compared to a standard-processed hypo-eutectic HMS material with a similar particle fraction (microstructure shown in Ref. [6]), the reduced and more homogeneous size and distribution of particles did not translate into improved tensile properties, but the toughness is strongly improved from 1.87 to 4.21 J $cm^{-2}$.

## 5. Discussion

Fe – $TiB_2$ based HMS can be readily synthesised by liquid metallurgical methods, i.e. conventional melting and casting procedures (Fig. 2a). The main challenge for enabling HMS as the next generation of mass-produced lightweight materials, however, lies in overcoming the inherent conflict between mechanical performance (i.e. strength and ductility) and physical properties (i.e. $E$ and $\rho$). The latter depend mainly on the particle fraction (Fig. 1b [11]), the former on the resultant morphology, size and dispersion of the particles, determined by the alloy composition and processing conditions [27].

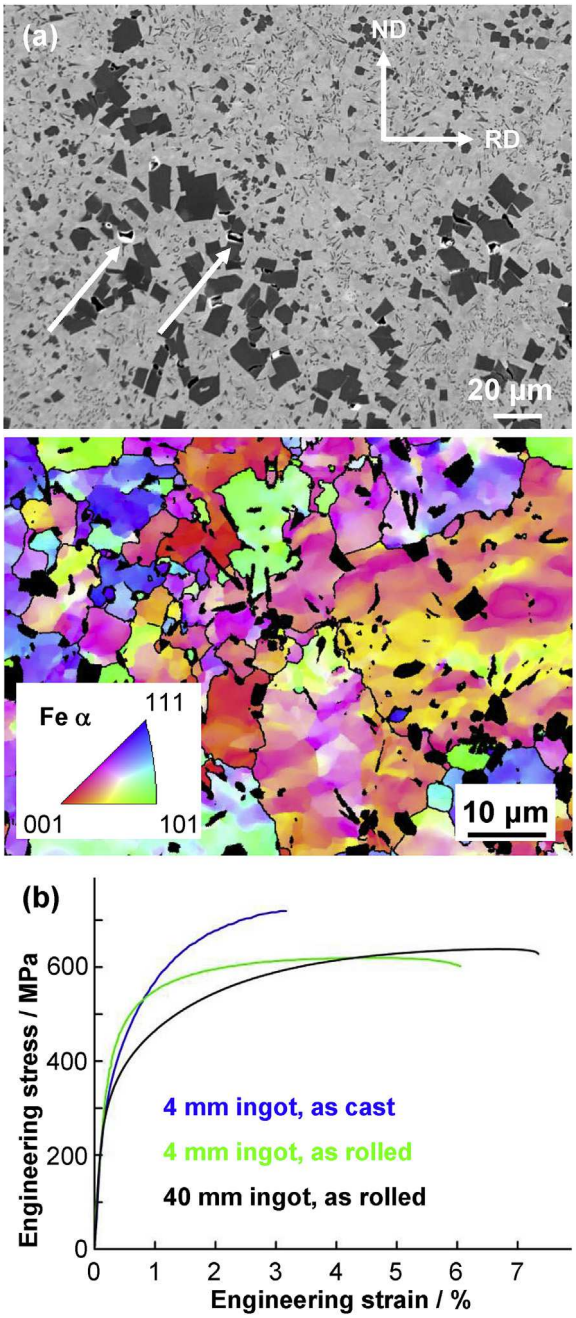


**Fig. 5.** Effect of hot rolling on the microstructure and mechanical properties of a High Modulus Steel with 20 vol% $TiB_2$ cast into a 4 mm thick mould: SEM image and EBSD IPF map (a) and tensile curves (b).

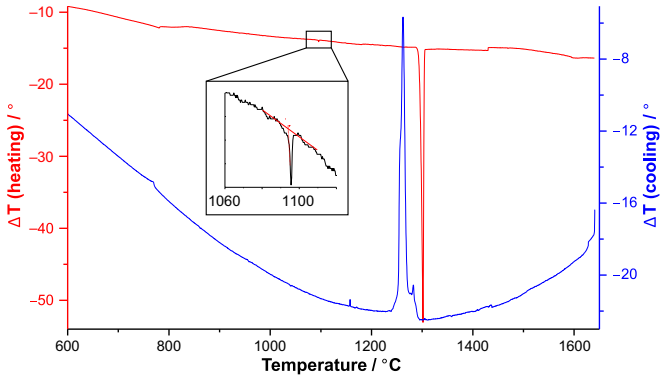


**Fig. 6.** Differential thermal analysis results for heating and cooling a High Modulus Steel with 20 vol% $TiB_2$ (stemming from casting into a 10 mm thick mould) to 1640 °C and back to room temperature. The differing temperatures of the corresponding peaks on the heating and cooling curve and the appearance of an additional peak close to the liquid-solid transition suggest a different composition profile during cooling as compared to that during heating.

As the $TiB_2$ particles are thermodynamically stable solidification products (Fig. 1a), the particle's microstructure is determined by the solidification conditions, and consequently conventional solid-state TMT such as hot rolling and annealing can not be used to significantly alter it. Hot rolling for instance cures casting defects such as pores in the matrix, but the respective rolling parameters (e.g. reduction, temperature etc.) need to be chosen carefully to avoid inducing new defects such cracks within the $TiB_2$ particles and at their sharp edges (Fig. 2b), in agreement to what has been reported by Rana et al. [15]. Especially the constitution of the matrix at the rolling temperature needs to be evaluated carefully, as the Fe-Ti-B phase diagram is still under refinement [25], and thus it is possible that for example unwanted ferrite may be present, affecting the matrix recrystallisation. Thus the mechanical properties of HMS can be improved by TMT procedures, but their general level is still unsatisfactory (Fig. 2c), especially in view of other high performance materials for lightweight design [28–30].

As improving the mechanical performance through alloying modifications does not only increase the production costs, but also potentially lowers the stiffness of the matrix (more ductile austenitic stainless steel has for example a lower specific modulus than ferrite [18]), it appears favourable to tailor the particle's microstructure through adequate solidification kinetics. Above an ingot thickness of about 40 mm the solidification rate is too slow to avoid strong floatation and clustering of primary particles induced by their lower density than the matrix. This is the case for industrial continuous casting with mould diameters of about 250 mm and a metallurgical length (i.e. liquid zone) of several meters [31], and consequently only hypo-eutectic HMS alloys can be produced in that manner. This phenomenon is attenuated by decreasing the mould thickness, but the size of $TiB_2$ particles drops only slightly until sample thicknesses of about 5 mm (Fig. 4a) and does not translate into improved mechanical properties (Fig. 5b).

With further decreasing mould thickness, the solidification is fast enough to limit growth and favour nucleation of $TiB_2$, as the primary particles become continuously smaller to about half their size at 1 mm thick casts, and the eutectic particles degenerate from lamellar to a fine network-type structure (Fig. 4c). In parallel, the grain size of the ferrite matrix is refined as well (Fig. 4b). We approximated the solidification rate of Fe – $TiB_2$ HMS by a Newton's law of cooling (taking the heat transfer from liquid to solid via convection as rate controlling [32]) based on experimentally determined values [6]. As shown in Fig. 9, the strong increase of the cooling rate coincides with the accelerated decrease in primary particle size at a mould thickness of about 4 mm. Based on these findings, the critical cooling rate in the upper temperature regime (i.e. solidification) for particle refinement in HMS appears to be about 60 K $s^{-1}$. Below a mould thickness of about 1 mm, the formation of eutectic particles (i.e. the constituent with the lowest melting point) is becoming suppressed, which is in agreement with observations for bulk metallic glasses of similar composition [33]. Suppression of primary particles needs an even faster cooling rate only achievable in sample thicknesses below about 100 µm [6]. However, material thicknesses below 4 mm require adapted production strategies such as strip-casting [29]; and TMT to tune matrix grain size is difficult to be performed reliably (too little reduction possible). Thus, the refinement of particle microstructure

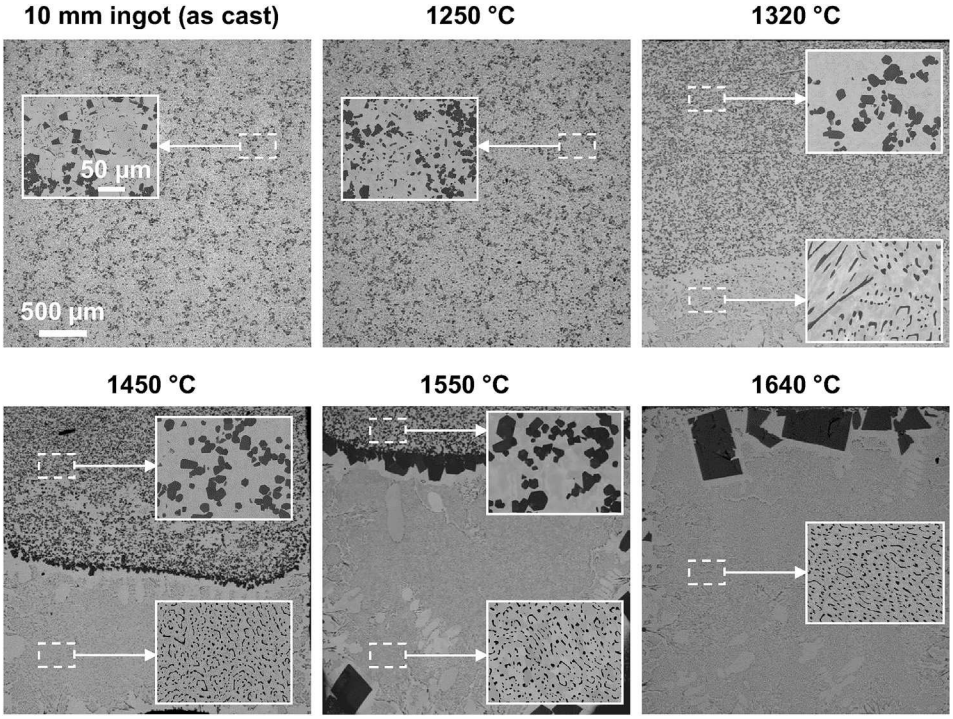


**Fig. 7.** SEM images visualising the effect of reheating temperature on the microstructure of a High Modulus Steel with 20 vol% $TiB_2$ (Differential thermal analysis samples, taken from casting into a 10 mm thick mould).

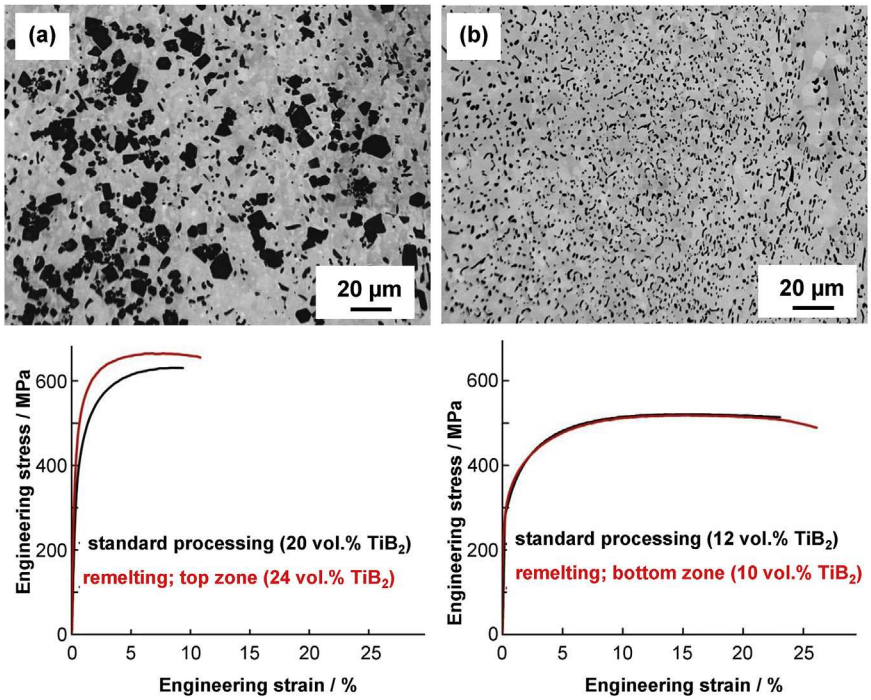


**Fig. 8.** Exploitation of the density-induced separation of primary and eutectic $TiB_2$ particles through remelting and slow solidification: (a) microstructure and tensile properties of the top zone with a higher fraction of mainly primary particles, (b) respective data for a purely eutectic bottom zone.

achievable by rapid solidification requires alternative synthesis techniques such as spray compaction [34] and other liquid metal deposition processes (e.g. Laser based techniques). Ti and B solutes in the matrix from suppressed eutectic decomposition can be utilised for nano-scaled precipitation of $TiB_2$ during subsequent TMT [6].

Even though these routes are extremely promising for HMS with optimum particle morphologies and dispersion (and thus mechanical properties), synthesis by decelerated solidification appears to be more promising for volume production. Instead of continuous strip-casting, slow solidification as in large-scale block casting (with a solidification rate below about 1 K $s^{-1}$) allows all primary

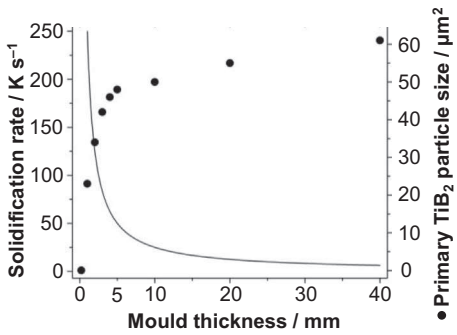


**Fig. 9.** Approximated solidification rate and primary $TiB_2$ particle size of a High Modulus Steel with 20 vol% $TiB_2$ as a function of the mould thickness.

particles to flow to the top of the melt, from which they can be easily removed either in the solid or liquid state, leaving a substantial amount of bulk material consisting exclusively of a spheroidised eutectic microstructure. Such material does not have the maximum physical property profile (eutectic fraction about 12 vol% $TiB_2$), and exhibits similar tensile behaviour as standard processed eutectic alloys (Fig. 8) as proposed elsewhere [35]. However, it possesses a much higher impact toughness, which is one of the key factors for thick-slab, heavy gauge materials (required f. e. for high performance cranes [36]) and enables more reliable production, as the alloy composition can be kept just above the eutectic concentration without risking either coarse primary particles (reducing ductility) or particle free ferritic zones (reducing the specific modulus). The resultant properties, of about 510 MPa UTS and more than 25% tensile elongation, reach the level of first generation advanced high strength steels, but are of course further tuneable by alloying additions. At a specific modulus of about 30 GPa $g^{-1}$ $cm^3$ such purely spheroidised eutectic HMS represent thus extremely promising candidates for HMS design.

Even more interesting from an alloy design point of view is the route of utilising the density-induced phase separation taking place at annealing between solidus- and liquidus-temperature, even though it results in higher production efforts. It allows creating materials consisting exclusively of primary particles without eutectic lamellae in between, thus increasing the effective particle spacing (Fig. 8). Similar as in grey cast Fe alloys, where additions of for instance magnesium change the graphite flakes to spheres, an increase in ductility can be achieved [36], whereas the toughness in our case is slightly lowered. This is especially remarkable in the current case, as it occurs not only simultaneously with improved strength, but also goes hand in hand with an increase in particle fraction. Thus the inherent detrimental relationship between mechanical and physical properties can be overcome, resulting in a unique combination of a specific modulus of about 35 GPa $g^{-1}$ $cm^3$ at more than 650 MPa UTS and 12% tensile ductility. It appears best to apply this partial re-melting procedure on materials stemming from fast solidification (such as a 5 mm thick slab casts), as the primary particles are then small and not clustered. The material in the bottom of the annealed sample is not lost but usable for purely eutectic HMS as discussed above. In all cases, possible segregation of additional alloying elements (added to further improve the mechanical properties) of different density, as e.g. Al or Si, needs to be taken into account – as well as their effect on the eutectic $TiB_2$ concentration and temperatures – when the gravity-induced separation is utilised to refine the particle microstructure of HMS. The effect of gravity may also be assisted by electromagnetic forces as shown by Antoni-Zdziobek et al. [27]. It should be highlighted as well, as the comparatively low toughness data suggests, HMS samples are sensitive to the testing conditions, and thus the mechanical properties (especially ductility and toughness) can be affected by the surface conditions or the sample size. The data shown here was derived from small scale testing, and thus represents conservative values.

## 6. Summary and conclusions

In this study we investigated how the mechanical properties of liquid metallurgy produced Fe – $TiB_2$ based HMS can be improved by controlled solidification kinetics and subsequent hot rolling and annealing above the solidus-temperature. We systematically varied the solidification rate by casting into Cu moulds with diameters between 0.1 and 40 mm focussing on hyper-eutectic alloys (20 vol% $TiB_2$) for maximum physical performance, as specific modulus of HMS is determined by the volume fraction of $TiB_2$. The following conclusions can be drawn:

(1) Standard melting and casting procedures into ingots between 5 and 40 mm thickness results in irregular particle microstructure consisting of sharp-edged coarse primary particles (increasingly clustered with slower solidification) and closely spaced irregularly shaped eutectic lamellae. Casting defects can be alleviated by hot rolling, but as the effect of rolling on the particle's microstructure (i.e. size, morphology and dispersion) is limited, the mechanical properties (especially ductility) remain unsatisfactory.
(2) Increasing the solidification rate results only at mould diameters at around 4 mm (corresponding to a critical cooling rate of about 60 K $s^{-1}$) and below in a significant refinement of the particles' microstructure, necessitating alternative synthesis routes such as liquid metal deposition to utilise it for improved mechanical performance. Suppressed (eutectic) $TiB_2$ caused by the most rapid solidification can be finely precipitated in the matrix afterwards by annealing or hot rolling.
(3) Decreasing the solidification rate causes the less dense primary particles to float to the top of the cast sample, limiting thick-slab strip-casting of HMS to maximum eutectic concentrations. We thus propose to utilise block-casting instead (with a cooling rate of less than 1 K $s^{-1}$), as it readily allows removing the primary particles from the top of the cast, thus enabling large-scale reliable production of alloys with an optimum particle microstructure (purely spheroidised eutectic particles of about 1 µm in diameter) and consequently high ductility and especially superior toughness.
(4) Annealing of hyper-eutectic HMS just above the solidus-temperature (i.e. about 1450 °C) allows the eutectic zones to liquefy and sink, leaving only primary $TiB_2$ particles behind in the top of the alloy. Despite of the (locally) increased particle fraction (about 24 vol%), both strength and ductility are improved over standard processed HMS alloys with 20 vol% $TiB_2$.
(5) Future work is focussed on modelling the micromechanical phenomena occurring in deformation of HMS in order to derive knowledge-based guidelines for the further improvement of particle microstructures. Additionally, we aim at developing alloying strategies to further tailor the property profile of HMS, adapted to the presented solidification concepts.

## Acknowledgements

The support of M. Kulse and J. Wichert for synthesis and processing is gratefully acknowledged.

## References


[1] B. Park, W. Hwang, A facile fabrication method for corrosion-resistant micro/nanostructures on stainless steel surfaces with tunable wettability, Scr. Mater 113 (2016) 118–121.
[2] O.A. Zambrano, Y. Aguilar, J. Valdés, S.A. Rodriguez, J.J. Coronado, Effect of normal load on abrasive wear resistance and wear micromechanisms in FeMnAlC alloy and other austenitic steels, Wear 348–349 (2016) 61–68.
[3] M.H. Jang, J. Moon, J.Y. Kang, H.Y. Ha, B.G. Choi, T.H. Lee, C. Lee, Effect of tungsten addition on high-temperature properties and microstructure of alumina-forming austenitic heat-resistant steels, Mater. Sci. Eng. A 647 (2015) 163–169.
[4] Q. Zhou, L. Qian, L. Zhao, Q. Zhu, J. Meng, F. Zhang, Loading-rate dependence of fracture absorption energy of low-carbon carbide-free bainitic steel, J. Alloys Comp 650 (2015) 944–948.
[5] M.F. Ashby, Materials Selection in Mechanical Design, Butterworth-Heinemann, Burlington, MA, 2005.
[6] H. Springer, R. Aparicio-Fernandez, J. Duarte, A. Kostka, D. Raabe, Microstructure refinement for high modulus in-situ metal matrix composite steels via controlled solidification of the system Fe – $TiB_2$, Acta Mater 96 (2015) 47–56.
[7] F. Bonnet, V. Daeschler, G. Petitgand, High modulus steels: new requirement of automotive market. How to take up challenge? Can. Metall. Q. 53 (2014) 243–252.
[8] R.G. Munro, Material properties of titanium diboride, J. Res. Natl. Inst. Stand. Technol. 105 (2000) 709–720.
[9] A.K. Shurin, V.E. Panarin, Phase equilibria and structure of alloys Fe $TiB_2$, Fe $ZrB_2$, Fe $HfB_2$, Izv. Akad. Nauk. SSSR Met. 5 (1974) 235.
[10] L. Cha, S. Lartigue-Korinek, M. Walls, L. Mazerolles, Interface structure and chemistry in a novel steel-based composite Fe-TiB2 obtained by eutectic solidification, Acta Mater 60 (2012) 6382–6389.
[11] J.C. Halpiri, J.L. Kardos, The Halpin-Tsai equations: a review, Polym. Eng. Sci. 16 (1976) 344–352.
[12] M. Kuzmina, D. Ponge, D. Raabe, Grain boundary segregation engineering and austenite reversion turn embrittlement into toughness: example of a 9 wt.% medium Mn steel, Acta Mater 86 (2015) 182–192.
[13] D. Raabe, D. Ponge, O. Dmitrieva, B. Sander, Nanoprecipitate-hardened 1.5 GPa steels with unexpected high ductility, Scr. Mater 60 (2009) 1141–1144.
[14] R. Aparicio-Fernández, H. Springer, A. Szczepaniak, H. Zhang, D. Raabe, In-situ metal matrix composite steels: effect of alloying and annealing on morphology, structure and mechanical properties of $TiB_2$ particle containing high modulus steels, Acta Mater. 107 (2016) 38–48.
[15] S. Lartigue-Korinek, M. Walls, N. Haneche, L. Cha, L. Mazerolles, F. Bonnet, Interfaces and defects in a successfully hot-rolled steel-based composite Fe-TiB2, Acta Mater. 98 (2015) 297–305.
[16] T.V. Pirtovsek, G. Kugler, M. Tercelj, The behaviour of the carbides of ledeburitic AISI D2 tool steel during multiple hot deformation cycles, Mater. Charact. 83 (2013) 97–108.
[17] R. Rana, C. Liu, Effects of ceramic particles and composition on elastic modulus of low density steels for automotive applications, Can. Metall. Q. 53 (2014) 300–316.
[18] M. Dammak, M. Gaspérini, D.Barbier. Microstructural evolution of iron based metal–matrix composites submitted to simple shear, Mater. Sci. Eng. A 616 (2014) 123.
[19] K. Tanaka, T. Saito, Phase equilibria in TiB2 reinforced high modulus steel, J. Phase Equilib. 20 (1999) 207.
[20] A.G. Gillen, B. Cantor, Photocalorimetric cooling rate measurements on a Ni-5 wt% A1 alloy rapidly solidified by melt spinning, Acta Metall. 33 (1985) 1813–1825.
[21] G.W.H. Höhne, H.K. Cammenga, W. Eysel, E. Gmelin, W. Hemminger, The temperature calibration of scanning calorimeters, Thermochem. Acta 160 (1990) 1–12.
[22] F. Stein, M. Palm, Re-determination of transition temperatures in the Fe-Al system by differential thermal analysis, Int. J. Mater. Res. 98 (2007) 580.
[23] S. Münstermann, W. Bleck, Influences on the elastic modulus of car body steels, Mater. Meas. 47 (2005) 337.
[24] N. Chawla, R.S. Sidhu, V.V. Ganesh, Three-dimensional visualization and microstructure-based modeling of deformation in particle-reinforced composites, Acta Mater 54 (2006) 1541–1548.
[25] Z. Hadjem-Hamouche, J.-P. Chevalier, Y. Cui, F. Bonnet, Deformation behaviour and damage evaluation in a new $TiB_2$ steel based composite, Steel Res. Intern. 83 (2012) 538.
[26] K.U. Kainer, Metallische Verbundstoffe, Vch Verlagsgesellschaft, 2003.
[27] A. Antoni-Zdziobek, M. Gospodinova, F. Bonnet, F. Hodaj, Solidification paths in the iron-rich part of the Fe-Ti-B ternary System, J. Alloys Compd. 657 (2016) 302–312.
[28] S. Kim, H. Kim, N.J. Kim, Brittle intermetallic compound makes ultrastrong low density steel with large ductility, Nature 518 (2015) 77.
[29] P. Hu, D. Shi, L. Ying, G. Shen, W. Liu, The finite element analysis of ductile damage. during hot stamping of 22MnB5 steel, Mater. Des. 69 (2015) 141–152.
[30] Yuly V. Milman, High-strength aluminum alloys, in: Oleg N. Senkov, Daniel B. Miracle, Sergey A. Firstov (Eds.), Metallic Materials with High Structural Efficiency. V NATO Science Series II (146): Mathematics, Physics and Chemistry 139-150, Springer, Netherlands, 2004.
[31] N. Zapuskalov, Comparison of continuous strip casting with conventional technology, ISIJ Int. 43 (2003) 1115–1127.
[32] J. Szekely, N.J. Thermelis, Rate Phenomena in Process Metallurgy, John Wiley & Sons Inc, 1971.
[33] A. Inoue, Stabilization of metallic supercooled liquid and bulk amorphous alloys, Acta Mater 48 (2000) 279.
[34] V.C. Srivastava, N. Ellendt, C. Meyer, V. Uhlenwinkel, Synthesis of bulk amorphous and nano-crystalline materials by spray forming, in: SDMA2013, September 23-25, Germany, Bremen, 2013.
[35] Arcelor Research group, Patent EP 1 897 963 A1, Bulletin, 2008, p. 20.
[36] H. Berns, W. Theisen, Eisenwerkstoffe: Stahl und Gusseisen, Springer Verlag, Berlin, Heidelberg, 2006.